The Chalmers Cloud Ice Climatology: A Novel Robust Climate Record of Frozen Cloud Hydrometeor Concentrations

JGR Atmospheres

RESEARCH ARTICLE
10.1029/2024JD042618

The Chalmers Cloud Ice Climatology: A Novel Robust Climate Record of Frozen Cloud Hydrometeor Concentrations

Simon Pfreundschuh[1], Julia Kukulies[2], Adrià Amell[3], Hanna Hallborn[3], Eleanor May[3], and Patrick Eriksson[3]

[1]Colorado State University, Fort Collins, CO, USA, [2]NSF National Center for Atmospheric Research, Boulder, CO, USA, [3]Chalmers University of Technology, Gothenburg, Sweden

Key Points:

- The Chalmers Cloud Ice Climatology (CCIC) provides the currently most accurate long-term record of TIWP compared to CloudSat/CALIPSO-based reference estimates
- The time series of global mean TIWP estimates from CCIC is stable over 40 years of observations
- 40 year trends indicate increasing TIWP over Southern Ocean and east Bering Sea in three out of four assessed data sets

Correspondence to:

S. Pfreundschuh,
simon.pfreundschuh@colostate.edu

Citation:

Pfreundschuh, S., Kukulies, J., Amell, A., Hallborn, H., May, E., & Eriksson, P. (2025). The chalmers cloud ice climatology: A novel robust climate record of frozen cloud hydrometeor concentrations. *Journal of Geophysical Research: Atmospheres*, *130*, e2024JD042618. https://doi.org/10.1029/2024JD042618

Received 1 OCT 2024
Accepted 24 FEB 2025

Author Contributions:

Conceptualization: Simon Pfreundschuh, Julia Kukulies, Adrià Amell, Hanna Hallborn, Eleanor May, Patrick Eriksson
Formal analysis: Simon Pfreundschuh, Julia Kukulies, Adrià Amell, Hanna Hallborn, Eleanor May
Funding acquisition: Patrick Eriksson
Investigation: Simon Pfreundschuh, Julia Kukulies, Adrià Amell, Hanna Hallborn, Eleanor May
Methodology: Simon Pfreundschuh, Julia Kukulies, Adrià Amell, Hanna Hallborn, Eleanor May, Patrick Eriksson
Project administration: Simon Pfreundschuh
Software: Simon Pfreundschuh, Julia Kukulies, Adrià Amell, Hanna Hallborn, Eleanor May

Abstract Frozen cloud particles are an important component of the hydrological cycle and significantly influence the Earth's energy budget. Despite their important role, observational records constraining concentrations of atmospheric ice remain severely limited. Although combined radar and lidar estimates from the CloudSat and CALIPSO missions offer over a decade of high-quality data on ice hydrometeor concentrations, these estimates remain sparse. In contrast, products derived from passive satellite sensors typically provide better spatiotemporal coverage but disagree with CloudSat-based measurements. To address these limitations, we present a novel climate data record of total ice water path (TIWP), the Chalmers Cloud Ice Climatology (CCIC). It spans 40 years, from 1983 to the present, covering latitudes from 70° S to 70° N. CCIC offers TIWP estimates at three-hourly resolution from 1983 and half-hourly resolution from 2000 onwards. We demonstrate the long-term stability of CCIC by directly comparing it with CloudSat/CALIPSO-based estimates over the entire mission lifetime. Additionally, we assess CCIC against other long-term TIWP records, revealing that CCIC yields the most accurate TIWP estimates compared to CloudSat/CALIPSO-based reference estimates. Analysis of regional 40 year trends across four long-term TIWP data sets indicates an increase of TIWP over the Southern Ocean and the east Bering Sea in two observational data sets and ERA5. The CCIC climate record closes the gap between existing long-term TIWP records and CloudSat/CALIPSO-based reference measurements. The estimates' continuous coverage and demonstrated accuracy make it a valuable resource for lifecycle studies of storms and the analysis of fine-scale cloud features in a changing climate.

Plain Language Summary This study focuses on cloud ice observations for better understanding weather and climate. Cloud ice particles are formed in storms and play an important role in the transport of water from the atmosphere to the surface. Moreover, ice particles affect how energy is balanced in the Earth's atmosphere. To improve climate models, it is crucial to measure the concentration of these ice particles. Currently, observational data on cloud ice are limited. Although the satellite missions CloudSat and CALIPSO provide detailed information, their coverage is not comprehensive. Other satellite data sets provide better coverage but often disagree with the more precise radar and lidar data from CloudSat and CALIPSO. To address these issues, we created the Chalmers Cloud Ice Climatology (CCIC), a new data set that provides estimates of the vertically integrated ice concentrations, the total ice water path (TIWP), for the last 40 years. This data set offers high-resolution estimates and shows the best agreement with reference measurements from CloudSat/CALIPSO among currently available TIWP records. CCIC fills an important gap in available TIWP data sets, making it a valuable tool for studying storms and understanding how clouds are changing in a warming climate.

1. Introduction

Ice clouds are important components of the Earth's weather and climate. High concentrations of frozen hydrometeors occurring in convective storms are linked to the dynamics of the atmosphere and the global rainfall distribution (Bony et al., 2015). At the same time, spatially extensive high-level ice clouds significantly affect the Earth's radiative energy budget by modulating top of the atmosphere longwave radiative fluxes (Chen et al., 2000). Because of the importance of atmospheric ice in several weather- and climate-relevant processes, the concentration of ice hydrometeors, the ice water content, and its vertical integral, the ice water path (IWP) have been identified as crucial parameters for improving climate models and quantifying climate sensitivity (Waliser et al., 2009). Although weather and climate models move toward higher spatial resolution and the explicit

Supervision: Patrick Eriksson
Validation: Simon Pfreundschuh, Julia Kukulies, Adrià Amell, Hanna Hallborn, Eleanor May
Visualization: Simon Pfreundschuh, Julia Kukulies
Writing – original draft: Simon Pfreundschuh, Julia Kukulies
Writing – review & editing: Simon Pfreundschuh, Julia Kukulies, Adrià Amell, Hanna Hallborn, Eleanor May, Patrick Eriksson

representation of convective processes at kilometer scales (Lucas-Picher et al., 2021; Prein et al., 2015), the representation of ice clouds in these models remains challenging (Feng et al., 2023; Turbeville et al., 2022).

A critical prerequisite for improving the representation of ice clouds in models is a robust observational record that accurately constrains atmospheric ice concentrations (Waliser et al., 2009). Although the vertically resolved synergistic observations afforded by the CloudSat and CALIPSO missions have ushered in a new era of cloud remote sensing (Stephens et al., 2002), the limited spatial and temporal sampling of the observations leaves crucial gaps in the observational record. Moreover, significant discrepancies between different satellite records and reanalysis data sets of IWP have been highlighted by Eliasson et al. (2011) and later reaffirmed by Duncan and Eriksson (2018).

Some of the longest available records of cloud water path date back to 1983 and come from the International Satellite Cloud Climatology Project (ISCCP, Rossow & Schiffer, 1999) and Pathfinder Atmospheres—Extended (PATMOS-x, M. J. Foster et al., 2023) data sets. The cloud water path estimates can be combined with cloud phase information to derive estimates of IWP. However, the IWP estimates provided by ISCCP and PATMOS-x have significant limitations. They are restricted to daytime measurements, and there are no validation studies assessing the accuracy of these estimates. This is particularly concerning because Eliasson et al. (2011) found that zonal means of the IWP estimates of ISCCP are about a factor of three lower than those of PATMOS-x and deviate significantly from the radar-based CloudSat estimates. The Moderate Resolution Imaging Spectroradiometer (MODIS) cloud properties product (Platnick et al., 2016) represents another important global long-term record of IWP. However, the MODIS IWP estimates are also limited to daytime estimates and lack independent validation. Moreover, Duncan and Eriksson (2018) determined that MODIS underestimates combined radar-lidar retrievals of cloud ice by a factor of three.

As Duncan and Eriksson (2018) pointed out, a potential reason for the significant discrepancies between various IWP records and reanalysis data is the ambiguity surrounding whether these estimates include both precipitating and nonprecipitating ice particles or are limited to just one category. In this study, we focus on estimates including both precipitating and nonprecipitating ice particles, which we will denote as the total ice water path (TIWP). Since the observational data sets assessed here do not define whether their estimates correspond to precipitating or nonprecipitating ice particles nor provide a way to distinguish them, the practically most relevant approach is to take the provided IWP estimates to correspond to the TIWP.

The Chalmers Cloud Ice Climatology (CCIC) is a novel long-term climate record of TIWP estimates developed to address the shortcomings of existing observational TIWP data sets. CCIC provides continuous TIWP estimates, that is, during day and nighttime at a high temporal resolution of 3 h from 1983 until 2000 and 30min from 2000 until the present. Moreover, it is designed to match the combined radar-lidar TIWP estimates of the CloudSat 2C-ICE product. The CCIC record is based on the retrieval described and extensively validated by Amell et al. (2024). The retrieval leverages a state-of-the-art convolutional neural network (CNN) model trained on geostationary infrared (IR) observations collocated with CloudSat/CALIPSO-based TIWP estimates. Since the retrieval relies only on single-channel geostationary IR observations, CCIC can provide TIWP estimates for the full observational record of geostationary IR observations, which extends back until 1983 and is available continuously around much of the globe between 70° S and 70° N.

This study presents, validates, and analyzes the full CCIC TIWP record we recently produced and made publicly available through Amazon Web Services (https://registry.opendata.aws/ccic/). The two primary goals of this paper are: first, to demonstrate the stability of the CCIC record by validating it against TIWP estimates from combined CloudSat/CALIPSO observations; and second, to evaluate the ability of CCIC TIWP estimates to capture significant climate features, including global distribution, seasonal to interannual variability, and long-term trends. To achieve these objectives, we first validate the CCIC estimates against reference TIWP estimates from the CloudSat/CALIPSO missions and then compare CCIC to the primary long-term TIWP records in order to highlight the consistency and potential additional insights into climate variability provided by the novel CCIC record.

The remainder of this article is organized as follows. Section 2 presents the data sets upon which the study is based and details the preprocessing steps applied to each. Section 3 starts out by validating the CCIC estimates and comparing other currently available long-term TIWP records against CloudSat/CALIPSO-based reference estimates. Following this, global time series (Section 3.3), spatial distribution (Section 3.4), seasonal variability

(Section 3.5), and long-term trends (Section 3.6) in the CCIC records are assessed and compared to those from other long-term TIWP records. Finally, a discussion of the results is given in Section 4 and the main conclusions are summarized in Section 5.

2. Data and Methods

2.1. Reference TIWP Estimates

The central tenet of this study as well as the guiding philosophy behind CCIC is that spaceborne combined lidar-radar measurements of ice hydrometeor concentrations represent the best currently available estimates of the global distribution of total IWP. Consequently, we utilize the 2C-ICE (Deng et al., 2015) and DARDAR (Delanoë & Hogan, 2010) products, which are both derived from the same combined lidar and radar observations, as reference data sets to anchor the estimates of CCIC and the other long-term TIWP records evaluated in this study. We compare all TIWP estimates to both 2C-ICE and DARDAR in order capture some of the uncertainty in the CloudSat/CALIPSO-based reference estimates arising from modeling assumptions in the underlying retrieval methods.

To facilitate the comparison of CCIC and other data sets with the reference estimates, we prepare two TIWP time series for each of the evaluated data sets. The first set of time series, which we will refer to as the *matched time series*, is generated by collocating TIWP estimates from the long-term TIWP records with corresponding CloudSat/CALIPSO-based reference estimates. From the collocated estimates, the matched time series are computed using only measurements for which all considered long-term records produce valid TIWP estimates. This means that the matched time series comprises only daytime measurements (because of the limitations of the PATMOS-x, ISCCP, and MODIS records, and - from 2011 - CloudSat) within 60 °S and 60 °N (because of the limitation of the 30 min CCIC estimates). The strict collocation of the passive-sensor-based estimates with the radar/lidar observations ensures that the spatiotemporal sampling of the resulting time series is identical and the resulting time series can be compared directly and unambiguously.

The second set of time series, the *native time series* consists of the monthly means calculated using all available measurements from each record. These records will differ due to differences in the spatiotemporal sampling of the underlying estimates; however, the native time series allows us to compare the records outside of the lifetime of the CloudSat and CALIPSO missions. For the products without a monthly aggregate version, we create a time series of monthly distributions of TIWP by aggregating the derived TIWP estimates by month.

2.2. CCIC

The CCIC data records are produced from two distinct observational data sets yielding two separate sub-records designated as CCIC (GridSat) and CCIC (CPCIR). The CCIC (GridSat) data record utilizes IR window-channel observations from the GridSat-B1 product version 2 (K. R. Knapp et al., 2011) data set as input. In contrast, the CCIC (CPCIR) data record employs observations from the National Oceanic and Atmospheric Administration (NOAA) Climate Prediction Center's globally merged IR product version 1 (Janowiak et al., 2001, 2017). The two realizations of the CCIC record inherit temporal coverage and spatiotemporal resolution of their respective input data sets. Specifically, the CCIC (GridSat) data set spans from 1983 to the present with a spatial resolution of 0.07° and a temporal resolution of 3 hr. Meanwhile, the CCIC (CPCIR) data set covers the period from 2000 to the present, featuring a temporal resolution of 30 min and a spatial resolution of 0.036°.

Both the GridSat and CPCIR observations exhibit systematic gaps in spatial coverage particularly from 1983 to the early 2000s. To minimize the impact of changes in geographical coverage on aggregated time series of hydrometeor concentrations, we only consider areas with at least 90% coverage in the first two decades of the GridSat-B1 data set. These resulting spatial masks are displayed in Appendix A.

2.2.1. The CCIC Retrieval Model

The CCIC retrieval is based on a CNN trained to retrieve TIWP, total ice water content (TIWC), cloud mask, and cloud type. The only input data for the retrieval are spatially resolved IR window-channel observations from geostationary satellites. Individual retrievals are performed on input images of size 256 × 256 pixels on the regular latitude-longitude grids of the underlying CPCIR and GridSat-B1 data sets. Global retrievals are performed using a sliding-window technique with an overlap region of 128 pixels in which overlapping results are blended linearly. The training data for the TIWP and TIWC estimates are derived from the CloudSat 2C-ICE

product, which is based on combined radar and lidar observations. The retrieval was trained using data from the period 2006 to 2009 with data from 2010 being used for model evaluation. Comprehensive validation experiments presented by Amell et al. (2024) demonstrate the accuracy and robustness of the retrieval across various climate and cloud regimes.

2.3. ISCCP

ISCCP TIWP estimates are derived from the HGG and HGM data sets of the ISCCP H-Series data set (W. B. Knapp et al., 2016) providing 3-hourly and monthly estimates, respectively. Since the ISCCP data record does not contain an explicit TIWP variable, we derive the TIWP from the cloud type information and the cloud-type-specific water path. The TIWP is calculated as the sum of the cloud-type-specific water paths over all frozen cloud types scaled with each cloud type's relative contribution to the total cloud amount. Since the cloud-type-specific water content is only available during daytime, the TIWP estimates are also limited to day-time measurements. The matched time series for ISCCP were produced by interpolating the 3-hourly estimates to the corresponding CloudSat measurements using nearest-neighbor interpolation.

2.4. PATMOS-X

The PATMOS-x (M. J. Foster et al., 2021) record provides in-cloud estimates of the total water path only during daytime conditions. In order to convert these estimates to all-sky TIWP estimates, we use the cloud phase information to identify ice clouds. Since PATMOS-x contains missing values in both no-cloud and nighttime conditions, it was necessary to use the daytime flag to identify no-cloud conditions.

PATMOS-x data are provided in daily files separately for each sensor. As for all other data sets considered here, we derive two records from the PATMOS-x data. To create the matched time series, we select the estimates from the sensor that are closest in time to the CloudSat/CALIPSO estimates, limiting the maximum time difference between overpass and CloudSat estimates to 3 hr. Moreover, we create the native time series by aggregating all the daily TIWP estimates from all sensors to monthly averages.

2.5. MODIS

To derive the native TIWP time series for MODIS, we make use of the daily gridded level 3 product (Platnick, 2019). We aggregate the data to monthly means on the 1.0° latitude-longitude grid the data is provided on. Since the MODIS level 3 product contains in-cloud TIWP means, we derive all-sky TIWP estimates by weighing the TIWP by the ice cloud fraction. We generate the matched time series for MODIS from the MOD06-1KM-AUX product (CloudSat Project, 2018), which contains cloud retrieval results from the MODIS sensor on the Aqua satellite matched to the corresponding CloudSat rays.

2.6. ERA5

Although the ERA5 reanalysis is only partially based on observations through data assimilation, it provides a comprehensive global data set of a wide variety of physically consistent atmospheric variables (Hersbach et al., 2020). To compare the TIWP estimates from the aforementioned data sets with ERA5, we used the sum of the variables total column snow water (SIWP) and total column ice water (CIWP). It is important to note that these two 2D variables do not represent all frozen hydrometeors, as convective snowfall, produced by the cumulus parametrization scheme, is not included in the column-integrated values for atmospheric ice. Additionally, the ERA5 reanalysis is subjected to uncertainties arising from its forecasting system and parametrization schemes particularly for deep convective and microphysical processes that determine cloud type distributions and their associated hydrometeors. In contrast to satellite-based climate records of TIWP, the ERA5 data set is not a direct observational data set; however, it provides valuable context for understanding global frozen hydrometeor distributions, as these estimates are linked to simulated physical processes.

3. Results

3.1. Case Study

We begin the assessment of the CCIC data sets and the other long-term TIWP records against the CloudSat-based reference estimates with a case study of a CloudSat overpass over Typhoon Megi (05:22–05:29 UTC, 27

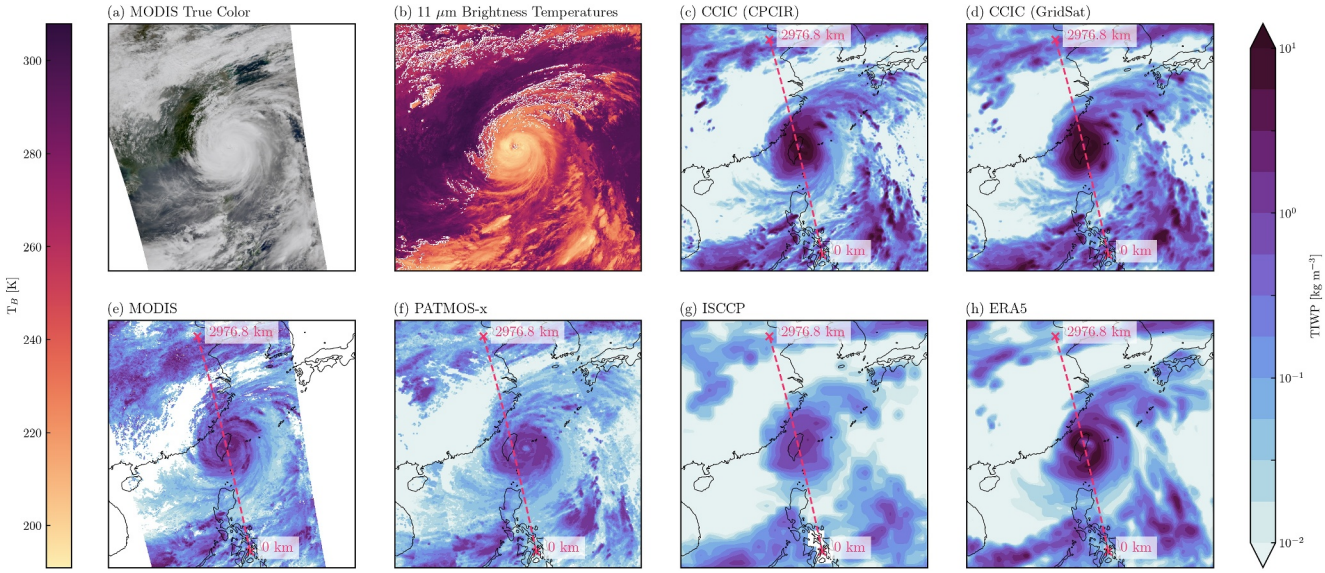

Figure 1. CloudSat overpass over Typhoon Megi, 05:22-05:29 UTC, 27 September 2016. Panel (a) shows a true-color composite derived from MODIS observations, Panel (b) shows the infrared window-channel observations used as input for the Chalmers Cloud Ice Climatology (CPCIR) retrieval, and Panel (c) to (h) show the TIWP estimates derived from the six long-term TIWP records assessed in this study.

September 2016). Figure 1 shows TIWP estimates from the six assessed long-term TIWP data sets: CCIC (CPCIR and GridSat), MODIS, PATMOS-x, ISCCP, and ERA5, alongside a MODIS true-color composite and 11 μm observations used as input for CCIC (CPCIR) retrievals.

The most obvious difference between the CCIC estimates and the other observational data sets is the magnitude of the TIWP around the center of the Typhoon with the CCIC estimates being about an order of magnitude higher than those from MODIS, PATMOS-x, and ISCCP. The CCIC (GridSat) estimates are less sharp than the CCIC (CPCIR) estimates, a consequence of the lower resolution of the input observations. Otherwise, however, the two CCIC estimates are in good agreement. The MODIS estimates exhibit the highest degree of spatial structure, a result of the high resolution of the sensor. At the same time, however, the estimates do not cover the full domain, illustrating another limitation of the MODIS record. The MODIS TIWP fields exhibit spatially more extensive ice cloud coverage but predict lower magnitudes than the CCIC records. The PATMOS-x TIWP field is very similar to the MODIS estimates but tends to produce even smaller TIWP estimates. The ISCCP estimates have the lowest spatial resolution of the assessed records and capture the overall position of the Typhoon but struggle to resolve the finer cloud structures in the scene. The ERA5 estimates are closest to the magnitudes produced by the CCIC retrievals but differ in terms of the internal structure of the Typhoon. Due to the comparably low resolution of the ERA5 estimates, the TIWP field is unable to resolve small-scale convective structures.

Figure 2 further compares the data sets along the CloudSat/CALIPSO ground track. CCIC (CPCIR) accurately captures the high TIWP concentrations at the storm center, lower TIWP in the anvil, and isolated convective cells south of the storm. CCIC (GridSat) results reproduce the large-scale TIWP structure but struggle to resolve the finer convective structures. ERA5 closely matches the CCIC data sets at the Typhoon center but isn't able to reproduce the finer cloud variability either. The MODIS TIWP estimates strongly underestimate TIWP concentrations at the storm center but show good agreement with 2C-ICE and DARDAR south of the storm. PATMOS-x, despite similarities to MODIS at broader scales, exhibits substantial deviations at finer scales. The closest PATMOS-x TIWP estimates for the overpass are about 3 hours old by the time of the overpass. The resulting time lag is likely to be an important source of uncertainty in the PATMOS-x estimates. ISCCP systematically underestimates TIWP across the scene and does not resolve small-scale convective features due to its coarse resolution.

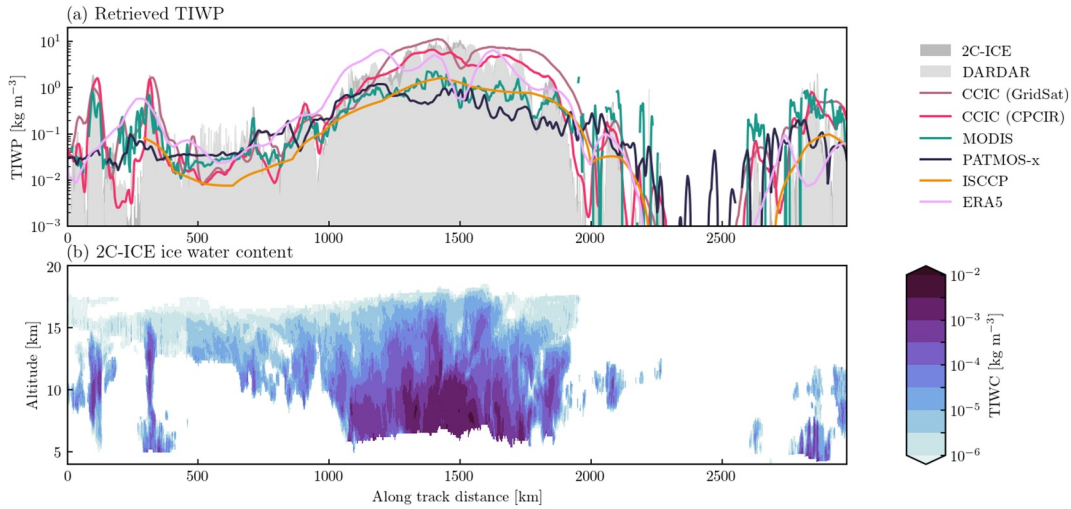

Figure 2. TIWP and total ice water content (TIWC) estimates along the CloudSat ground track for the Typhoon Megi overpass shown in Figure 1. Panel (a) displays reference TIWP estimates from the 2C-ICE and DARDAR products with the corresponding estimates from the long-term TIWP data sets interpolated to the CloudSat ground track. The areas under the plot lines corresponding to the 2C-ICE and DARDAR products are filled to make it easier to distinguish them from the other curves. Panel (b) shows the corresponding 2D field of ice water content from the 2C-ICE product.

3.2. Validation Against Combined Radar-Lidar Estimates

For a systematic analysis of the CCIC records and the other long-term TIWP data sets, we use the matched time series to assess the respective TIWP estimates with respect to reference data from the 2C-ICE and DARDAR products. Figure 3 shows time series of monthly averages of the matched TIWP estimates from the two CCIC records, 2C-ICE, and DARDAR as well as the other products assessed in this study. The CCIC estimates closely match those of 2C-ICE during the years 2006 until 2010, which have been used in the training of the retrieval, as well as the years after that. The 2C-ICE and CCIC estimates are about 20% higher than the estimates from the

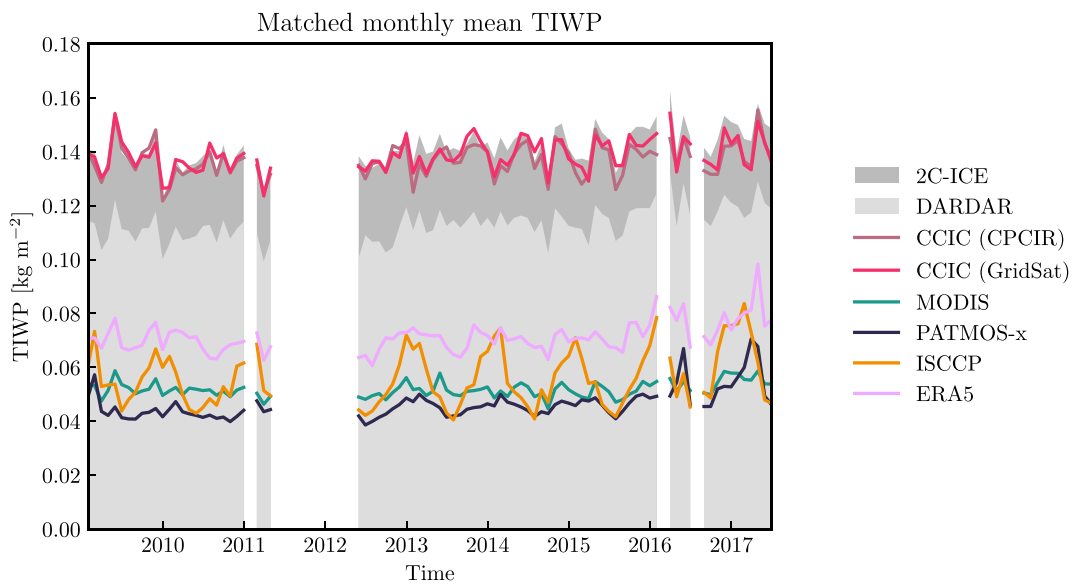

Figure 3. Monthly averages of matched TIWP estimates from all cloud products assessed in this study. All TIWP estimates were collocated to the CloudSat measurements and only collocations during daytime and within 60 °S and 60 °N in which all assessed products produce valid estimates are included in the calculation of the monthly means. The gaps in the time series are due to diminished operations of the CloudSat sensor in 2011, 2012, and 2016. The areas under the plot lines corresponding to the 2C-ICE and DARDAR products are filled to make it easier to distinguish them from the other curves.

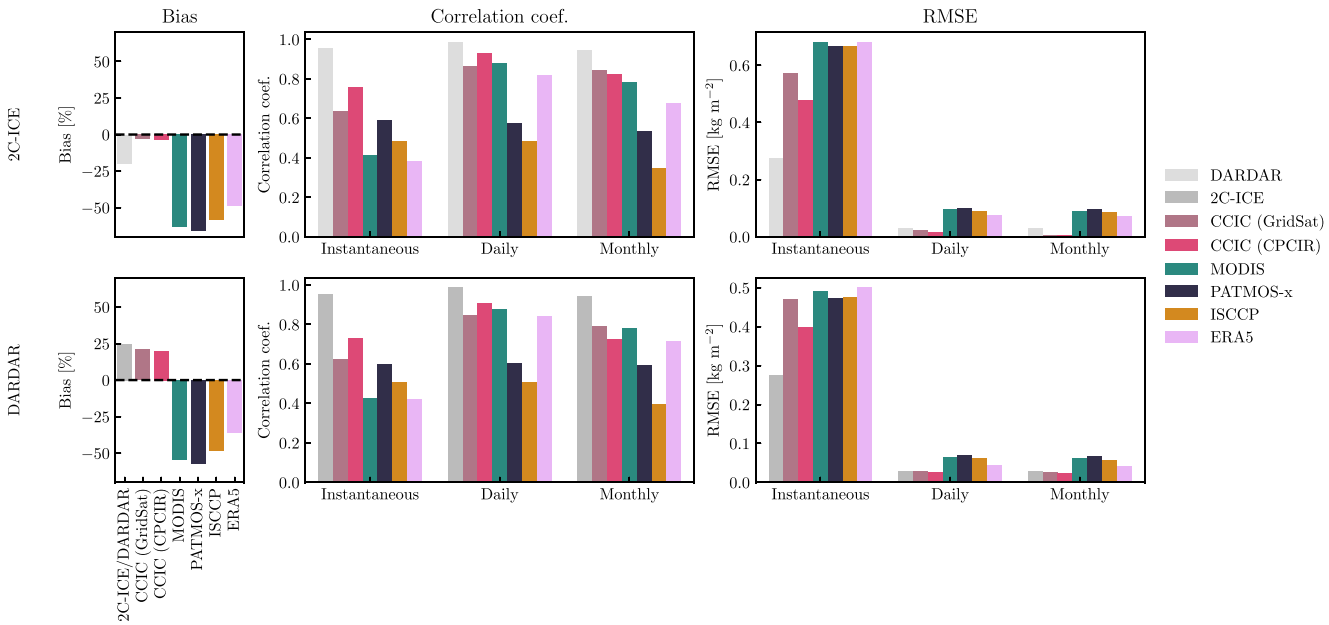

Figure 4. Validation statistics of the matched TIWP time series with respect to the 2C-ICE and DARDAR reference time series. The first row of panels shows the statistics calculated with respect to the 2C-ICE data. The second row of panels shows the statistics calculated with respect to the DARDAR data.

DARDAR product but the time series show a high degree of co-variability indicating that the products are consistent in terms of their monthly variability. In addition to the ISCCP estimates being lower than the 2C-ICE and DARDAR estimates, the monthly variability of this product does not align well with that of the reference estimates. The time series from the MODIS and PATMOS-x TIWP records are also significantly lower than both 2C-ICE and DARDAR. In terms of monthly variability, the MODIS estimates show better agreement with the reference estimates compared to the PATMOS-x time series.

To assess the accuracy of the CCIC records across multiple scales of temporal variability, Figure 4 displays the bias, correlation coefficient, and root mean squared error (RMSE) for instantaneous to monthly timescales with respect to the 2C-ICE and DARDAR reference data sets. The daily and monthly estimates were derived from the matched time series by averaging all valid estimates over the corresponding time intervals. The metrics were computed using only data outside the CCIC training and testing period 2006–2010. Both CCIC records exhibit small biases of the order of few percent compared to 2C-ICE and about a 20 % bias compared to DARDAR. The remaining records all exhibit fairly large negative biases of around 60 % compared to 2C-ICE and around 50 % compared to DARDAR.

For instantaneous estimates, the CCIC records exhibit the highest correlation with both the 2C-ICE and the DARDAR reference data followed by PATMOS-x, ISCCP, MODIS, and ERA5. The higher correlations of CCIC (CPCIR) compared to CCIC (GridSat) are likely due to the higher temporal resolutions of the CCIC (CPCIR) record. Since the CCIC (CPCIR) record has a temporal resolution of 30min, the average time between input observations and corresponding 2C-ICE and DARDAR reference estimates will be significantly lower than for CCIC (GridSat) estimates. In terms of RMSE with respect to 2C-ICE, the CCIC (CPCIR) and CCIC (GridSat) time series yield the smallest errors. Compared to DARDAR, the CCIC records still yield the smallest errors but the RMSE of the CCIC (GridSat) time series is close to the RMSE of the MODIS, PATMOS-x, and ERA5 records.

At daily timescales, the correlation for the CCIC (GridSat) and CCIC (CPCIR) data sets increases further exceeding 0.8 in relation to both reference records. The correlation of the MODIS time series also rises sharply for daily timescales, yielding values close to the CCIC (CPCIR) record and even surpassing the CPCIC (GridSat) record. The correlation of the ERA5 TIWP also increases notably but stays below the level of the CCIC and MODIS records. In contrast, the correlations of the PATMOS-x and ISCCP records do not improve and instead show a slight degradation. All records exhibit significantly smaller RMSE at daily timescales but the reduction is most significant for the CCIC records. Meanwhile, the MODIS records remain at the level of the PATMOS-x and ISCCP data sets.

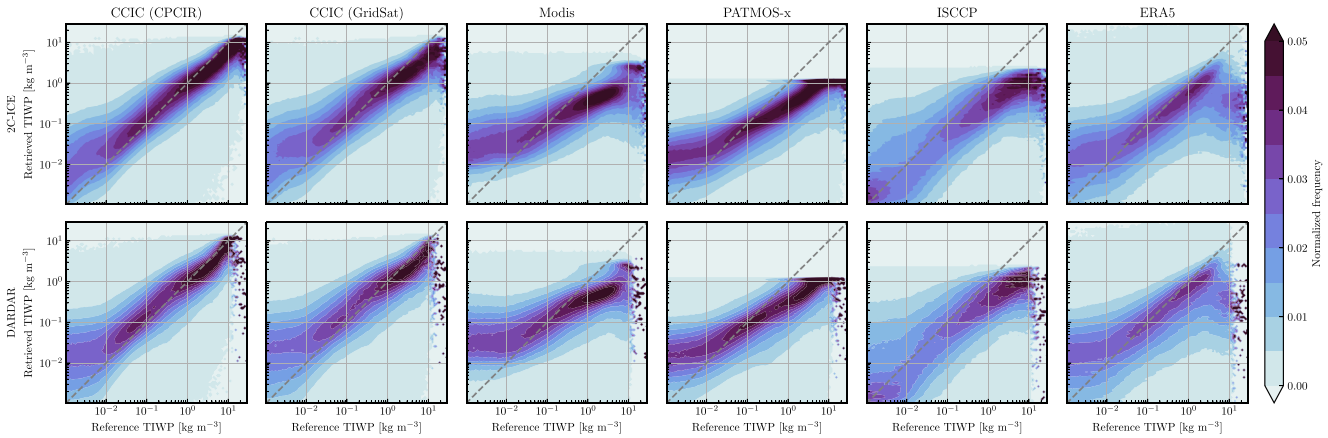

Figure 5. Scatter plots of reference and retrieved TIWP. Each panel shows the conditional distribution of retrieved TIWP with respect to the reference TIWP. The shading shows the relative frequency of each bin normalized by the total number of samples for the given reference TIWP bin. The first row shows the TIWP estimates compared to 2C-ICE reference estimates; the second row shows the corresponding results compared to DARDAR reference estimates. Columns show the results for the assessed long-term TIWP records.

At monthly timescales, the correlations of the CCIC and MODIS records decline but remain close to 0.8 compared to the 2C-ICE record. Compared to DARDAR, the degradation of the correlation of the CCIC records is more pronounced causing the CCIC (CPCIR) record to fall below that of the MODIS record while the CCIC (GridSat) record remains close to but slightly above the MODIS record. The correlations of the PATMOS-x and ISCCP records degrade even further compared to the correlation at daily timescales. Regarding RMSE, the errors for the CCIC records decrease further. The RMSEs of the other records remain at the same level as for daily timescale, indicating that the RMSEs at these timescales are dominated by systematic retrieval errors.

It is important to consider that the MODIS estimates have an inherent advantage due to the MODIS sensor being part of the A-train constellation. During the considered time period, the MODIS observations were nearly simultaneous with the CloudSat/CALIPSO reference measurements. In contrast, the other estimates exhibit notable time differences: up to 15 min for CCIC (CPCIR), 90 min for CCIC (GridSat) and ISCCP, and up to 180 min for PATMOS-x. These temporal discrepancies may affect the accuracy the non-MODIS estimates compared to MODIS.

To assess the retrieval accuracy across different cloud regimes, Figure 5 presents column-normalized scatter plots comparing reference and retrieved instantaneous TIWP estimates. The CCIC (CPCIR) retrievals exhibit the highest accuracy, demonstrating sensitivity to reference TIWP values ranging from 0.01 kgm^{-2} to 10 kgm^{-2} when compared to both 2C-ICE and DARDAR estimates. CCIC (GridSat) retrievals show slightly reduced accuracy and a narrower sensitivity range likely due to the lower temporal and spatial resolution of the underlying satellite imagery.

The remaining satellite-based estimates show significantly weaker agreement with the reference data particularly at high TIWP values. MODIS, PATMOS-x, and ISCCP fail to capture TIWP values exceeding 3 kgm^{-2}. Within the range of 0.05 kgm^{-2} to 0.5 kgm^{-2}, MODIS and PATMOS-x display relatively good agreement with the reference estimates, but their accuracy remains at the level of the CCIC retrievals despite the higher resolution and more comprehensive spectral coverage of the underlying observations. ISCCP and ERA5 records exhibit the largest spread around the diagonal likely due to their coarser spatial resolution. Additionally, ERA5 TIWP estimates exclude convective snow, contributing to the observed decrease in ERA5 TIWP values above 5 kgm^{-2}.

3.3. Global Mean TIWP

In order to assess the long-term stability of the TIWP records, we consider monthly means of each product's native time series. Figure 6 displays the monthly time series of area-weighted global mean TIWP for CCIC (GridSat) and CCIC (CPCIR) compared to the CloudSat/CALIPSO reference measurements and the other long-term records of atmospheric cloud ice. To reduce the effect of varying spatial coverage across time and data sets, the means displayed were calculated using the mask displayed in Figure A1.

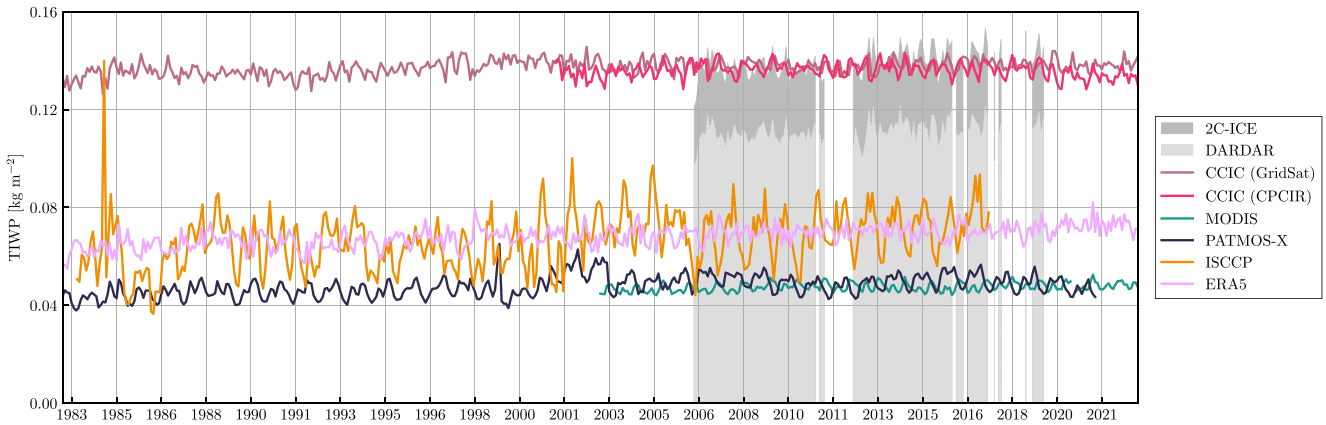

Figure 6. Native time series of monthly global mean TIWP for CCIC (GridSat) and CCIC (CPCIR) compared to other long-term TIWP records and ERA5. The global means are area-weighted and are spatially masked using the mask shown in Figure A1 to homogenize the spatial sampling across data sets. The areas under the plot lines corresponding to the 2C-ICE and DARDAR products are filled to make it easier to distinguish them from the other curves.

The data sets differ significantly in magnitude ranging from estimates around 0.05 kg m^{-2} to 0.15 kg m^{-2}. The global mean values of TIWP differ by a factor of three across the assessed observational data sets, which is in line with the discrepancies reported in previous studies (Duncan & Eriksson, 2018). Notably, the differences between the data sets exceed the seasonal and interannual differences. As for the matched time series shown in Figure 3, the CCIC estimates (CPCIR and GridSat) exhibit the highest global TIWP but align most closely with the two CloudSat-based reference products. Since the native CCIC time series comprise a larger number of estimates, they tend to exhibit less temporal variability than the 2C-ICE and DARDAR time series. The differences in temporal variability between the CCIC records and the CloudSat-based estimates increase after 2011 when CloudSat switches to daytime only operations. The lowest global TIWP estimates are found in the PATMOS-x and MODIS data sets. The native ISCCP estimates are significantly higher than for the matched time series (Figure 3), which is due to excessively high TIWP estimates between 60 and 70° N and S, which are included in the native time series but excluded from the matched time series. For the native time series, The MODIS estimates are slightly lower than the PATMOS-x estimates, which is the opposite of what was found for the matched time series (Figure 3). Also in this case, this difference between the matched and native time series is likely due to changes in the spatial coverage of the included results. Additionally, for the PATMOS-x data set, the native time series includes estimates from a larger variety of sensors whose retrieval results may differ due to changes in the spectral coverage of the sensors.

The CCIC (GridSat) time series is stable across the full 40 years of data availability. Where the CCIC (CPCIR) estimates are available they closely follow the CCIC (GridSat) estimates except at first and last 3 years of the CCIC (CPCIR) record where the estimates seem to diverge slightly. The MODIS time series is stable throughout its availability. The PATMOS-x record seems to exhibit a break point around 2001 with slightly increased mean TIWP after 2001. The ISCCP time series exhibits the strongest seasonal variability but also shows strong interannual variability, which seems unlikely to be physical given that it greatly exceeds the variability of the other records. A very strong anomaly is observed in 1984, which, upon inspection, was found to be caused by obvious retrieval errors. The ERA5 time series is stable in terms of interannual variability but seems to exhibit a weak but constant increasing trend.

3.4. Spatial Distribution

In addition to robust global mean estimates, a crucial feature of a global cloud ice climate record is its capacity to capture the spatial and temporal variability of TIWP. Therefore, we next asses the spatial and seasonal variability of the CCIC TIWP record in comparison to the CloudSat-based reference data sets and the other long-term TIWP records.

Figure 7 shows the spatial distributions of TIWP for each data set averaged over its respective full period of availability. As already established in the previous sections, the data sets differ significantly in magnitude with the DARDAR and 2C-ICE reference data sets and the CCIC data sets providing significantly higher TIWP values.

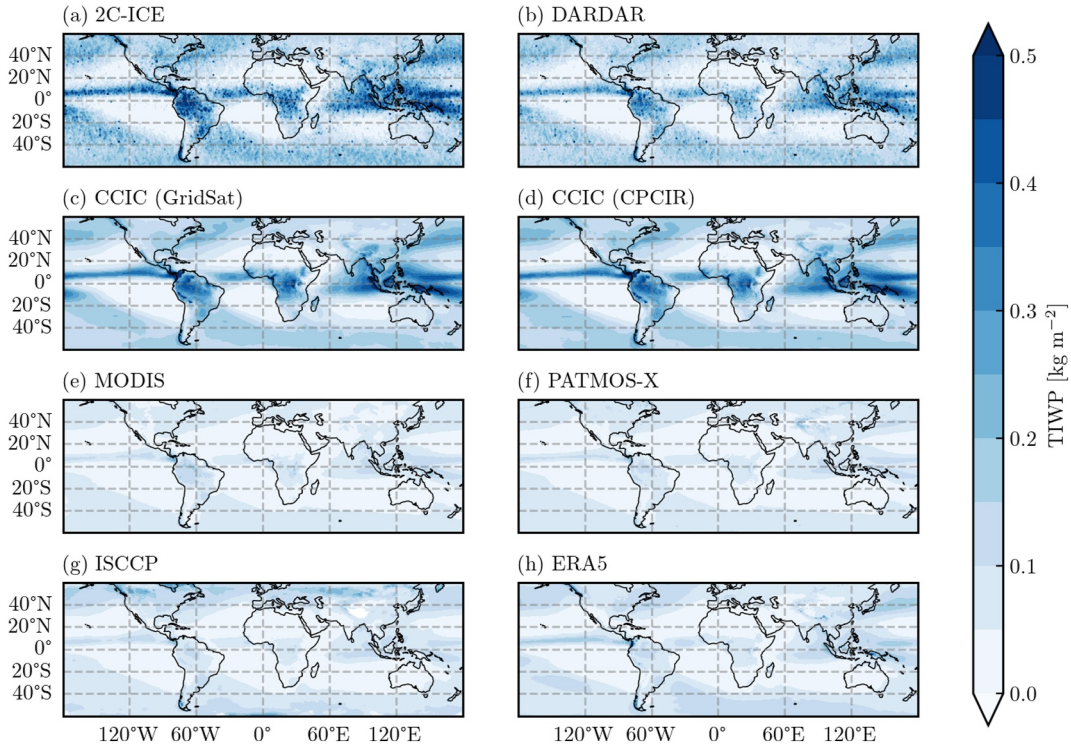

Figure 7. Global distribution of total ice water path (TIWP) for all assessed data sets (panels a–h). The distribution for each data set is calculated as the average over the full data record.

The differences are most evident in the tropical belt and the midlatitude storm tracks. Due to their much denser sampling compared to the 2C-ICE and DARDAR data sets, the CCIC data sets provide smoother global distributions resulting in more coherent spatial structures than the CloudSat-based measurements.

The MODIS, PATMOS-x, and ISCCP satellite-based TIWP records reproduce the principal features of the distribution apparent in the CloudSat-based records but strongly underestimate their magnitude. This underestimation is particularly strong in the tropics. ISCCP exhibits spurious TIWP peaks over high-latitude land surfaces that do not appear in the reference estimates and are therefore likely retrieval artifacts.

Figure 8 shows the corresponding zonal means for all data sets. The zonal means clearly illustrate the relative underestimation of the tropical TIWP concentrations compared to the midlatitude storm tracks in the MODIS, PATMOS-x, ISCCP, and ERA5 data sets. ISCCP, and, to a lesser extent, PATMOS-x exhibit dramatic increases toward higher latitudes suggesting that these data sets produce unrealistic TIWP values over snow and ice surfaces.

3.5. Seasonal Variability

Figure 9 shows the seasonal migration of TIWP for all considered data records. The normalized variability is very similar between all data sets. This indicates that cloud ice features that are linked to synoptic-scale climate variability are robustly captured by the different observational data sets despite their differences in magnitude.

Nonetheless, there are some finer-scale differences that show that CCIC may provide additional details that are not necessarily consistent among the data sets. In the tropics, the MODIS, PATMOS-x, and ISCCP data sets tend to slightly underestimate the magnitude of the variability, whereas it is overestimated in the ERA5 data. The CCIC data sets are closest to the CloudSat-based results.

In the northern-hemisphere midlatitudes, the CloudSat-based reference records exhibit a seasonal peak in January and February (light red). This is reproduced by all satellite records but occurs too late in the ERA5 data. The seasonal peak shifts to a peak in October to November at high latitudes. This shift is captured by both CCIC records and ERA5 but not the MODIS, PATMOS-x, and ISCCP records. In the southern hemisphere, the

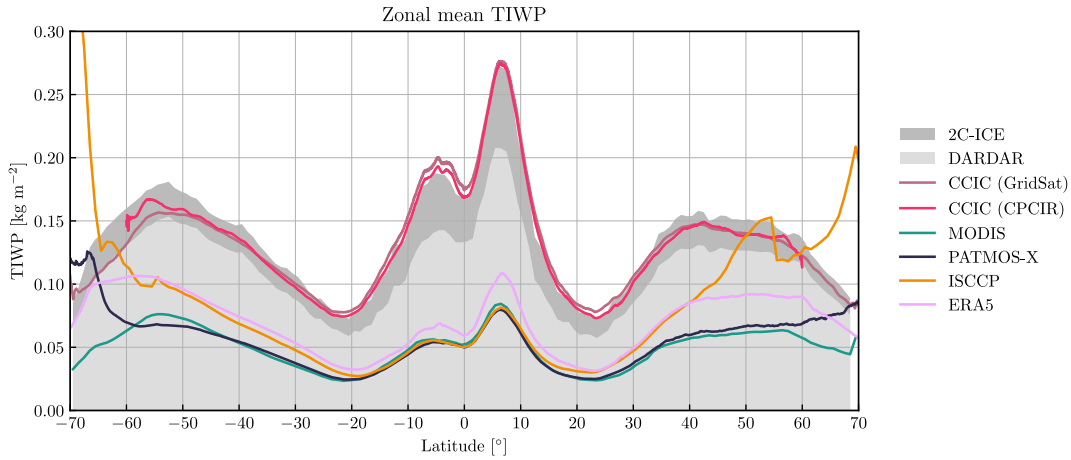

Figure 8. Zonal means of TIWP for the eight different data sets. The areas under the plot lines corresponding to the 2C-ICE and DARDAR products are filled to make it easier to distinguish them from the other curves.

midlatitude TIWP peak occurs in June and July. The shift of the peak toward March-April is visible in the CloudSat-based records but the seasonal cycle also becomes less pronounced. The shift is reproduced only in the MODIS and CCIC (GridSat) data sets.

3.6. Trend Analysis

In this section, we analyze regional long-term trends in TIWP. Since the CCIC (CPCIR) and MODIS data sets only start in the early 2000s, we split the analysis of the temporal TIWP trends into separate analyses of the 20 and 40 year trends starting in 1983 and 2003, respectively. At the time this analysis was performed, the ISCCP and PATMOS-x records were available only until 2018 and 2021, respectively. Therefore, the trends in these two data sets are calculated over slighty shorter time periods than the nominal 20 and 40 years.

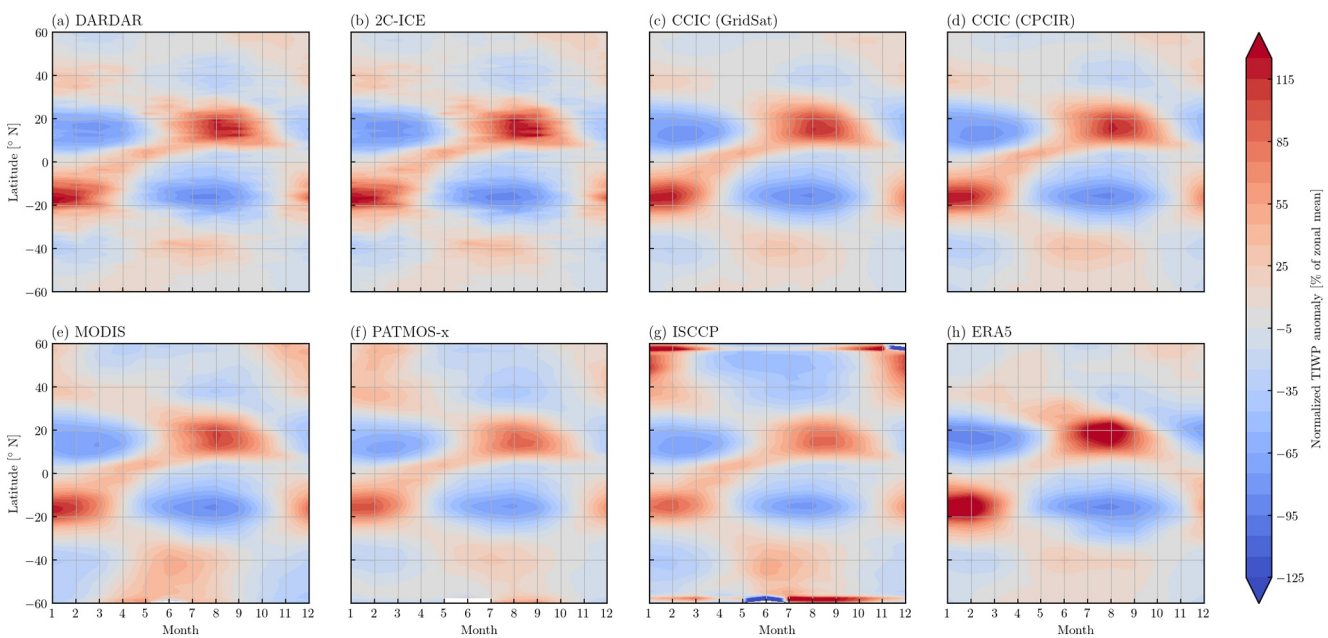

Figure 9. Hovmoller (time-latitude) diagrams of monthly TIWP anomalies over the full record of each of the data sets (panels a–h) and averaged over longitudes. The anomalies are normalized by latitude band using the corresponding zonal mean TIWP.

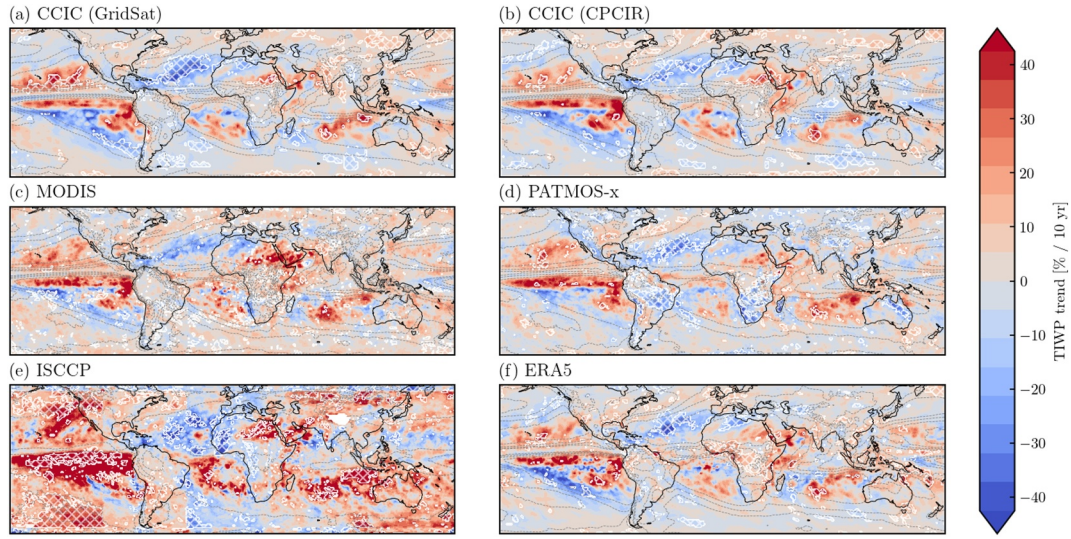

Figure 10. Decadal TIWP trends from 2003 to 2023 with respect to the grid cell level mean. Panels (a)–(f) display the results for the six assessed data sets. The spatial trend for each data set is based on the annual mean values in each grid cell for the full record. The red-shaded regions indicate an increase in TIWP, whereas the blue-shaded regions indicate a decrease in TIWP. Regions marked with white hatching indicate trends significant at the 95% confidence level.

3.6.1. 20-Year Trends

Figure 10 shows the spatial trends in the five passive sensor-based TIWP records and ERA5 for the time period 2003–2023. It is notable that the large-scale features of the trends are very consistent among the CCIC records, MODIS, PATMOS-x, and ERA5. The trends in ISCCP do not agree well with any of the other records and display clear sensor artifacts, such as the meridionally oriented discontinuities east of the Americas. Only few regions in the CCIC, MODIS, PATMOS-x, and ERA5 records exhibit statistically significant trends, indicating that the observed trends are driven by interannual variability rather than long-term climate trends. Nonetheless, these results indicate that the interannual variability is consistent between the CCIC, MODIS, PATMOS-x, and ERA5 records.

The MODIS TIWP record exhibits no cohesive areas of statistically significant TIWP trends. However, some regions of consistent trends can be observed in the CCIC, PATMOS-x, and ERA5 records. The largest of them is a negative trend observed over the subtropical North Atlantic. These areas of decreasing TIWP combined with scattered areas of significant increasing TIWP further north are indicative of a northward shift of the North Atlantic storm tracks. Additional areas of consistent significant trends can be found in the southern Indian Ocean and east of Hawaii.

3.6.2. 40-Year Trends

Figure 11 shows decadal trends for the four data records that allow the calculation of trends from 1983 until 2023 (or, 2018 and 2021 for ISCCP and PATMOS-x). As for the 20 year trends, the global structures of the trends between the CCIC, PATMOS-x, and ERA5 records are largely consistent.

Statistically significant increasing trends are observed over the Southern Ocean, the Bering sea, and the southern central Pacific. ERA5 and, to a lesser extent, PATMOS-x show significant increasing trends over the Inter-Tropical Convergence Zone (ITCZ) that are not present in the CCIC retrievals. However, with magnitudes exceeding 20 % per decade, at least the trends in the ERA5 data appear unrealistic. Over land there is little to no agreement between the three records. This indicates that retrieval uncertainties caused by land surfaces and cloud-surface interactions in ERA5 lead to discrepancies between the data records.

The CCIC (GridSat) trends exhibit an artifact over the Indian Ocean that is likely related to the missing observations throughout most of the first 20 years of the record (K. R. Knapp et al., 2011). Significant increasing trends over the Indian Ocean are also observed in the PATMOS-x and ERA5 records. Over the subtropical South Pacific,

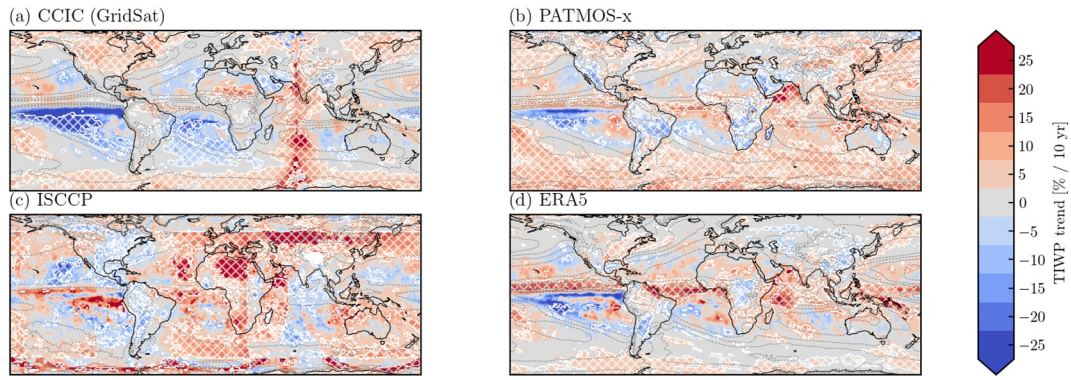

Figure 11. Decadal TIWP trends from 1983 to 2023 with respect to the grid cell level mean. Panels (a)–(d) show the means for the four assessed data sets. The spatial trend for each data set is based on the annual mean values in each grid cell for the full record. The red-shaded regions indicate an increase in TIWP, whereas the blue-shaded regions indicate a decrease in TIWP. Regions marked with white hatching indicate trends significant at the 95% confidence level.

the CCIC (GridSat) data show a very strong decreasing trend that is significantly weaker and less significant in PATMOS-x and ERA5. Although ERA5 and PATMOS-x also show some areas with significant negative trends in the South Pacific, they are smaller and interspersed with pockets of increasing trends.

The PATMOS-x record exibits increasing trends over most of the globe. This apparent bias toward increasing TIWP is conistent with the discontinuity in the global mean TIWP time series (Figure 6) occurring between 2000 and 2003, which is likely caused by changes in the observing system. The ISCCP trends exhibit the least resemblance to any of the other data sets and, as for the 20 year trends, are dominated by observations artifacts.

To provide a complimentary perspective on the evolution of TIWP in the four long-term TIWP records, Figure 12 displays 5 year meriodional and zonal mean curves for each of the data sets. The meridional means of the CCIC (GridSat) record show significant changes in the region between 50 and 100° E. Observations artifacts were visible in this regions also in the long-term trend maps (Figure 11) indicating that these features do not represent actual changes in the mean TWIP. The zonal means of CCIC (GridSat) indicate a strengthening in the northern hemisphere ITCZ but no consistent change in the southern hemisphere ITCZ. The storm tracks exhibit a strengthening and simultaneous poleward expansion. The meridional mean TIWP curves of the PATMOS-x reflect a continuous increase in TIWP over the Pacific and Indian ocean. The corresponding zonal means indicate that the strongest increases occurr in the northern hemisphere ITCZ, the storm tracks, and over high latitudes. The meridional means of ISCCP exhibit the most significant relative variability with a mostly irregular evolution over the east Pacific but a more consistent increasing trend over the rest of the globe. The zonal means indicate that the most significant changes occur in mid- and high-latitude regions. Finally, the ERA5 meridional means exibit the strongest changes over the Pacific and Indian Ocean. The zonal means reveal a significant increasing trend in the ERA5 ITCZ with the TIWP almost doubling over the 40 year period. Weaker changes are observed in the storm tracks, which exhibit a strengthening a poleward movement.

4. Discussion

4.1. Accuracy and Robustness of the CCIC Records

The primary aim of this study was to assess the accuracy and robustness of the CCIC climate records. Since the CCIC retrieval is based on a neural network trained using only data from 2006 until 2010, the robustness of the data record remained an open question. The validation results presented by Amell et al. (2024) extended outside the original training period and thus already provided preliminary evidence of the robustness of the retrievals. In this study, we provide a long-term assessment of the accuracy of the CCIC retrieval results. The evaluation of the CCIC TIWP estimates against the full available record of 2C-ICE and DARDAR based estimates demonstrates that the CCIC TIWP record provides robust estimates from 2011 until 2018. Moreover, the CCIC based estimates yield the most accurate results on instantaneous and daily timescales compared to other currently available long-term TIWP records. Even on monthly timescales the accuracy of CCIC (GridSat) remains on par with the MODIS based estimates despite being only based on observations from a single IR channel. It should also be noted that

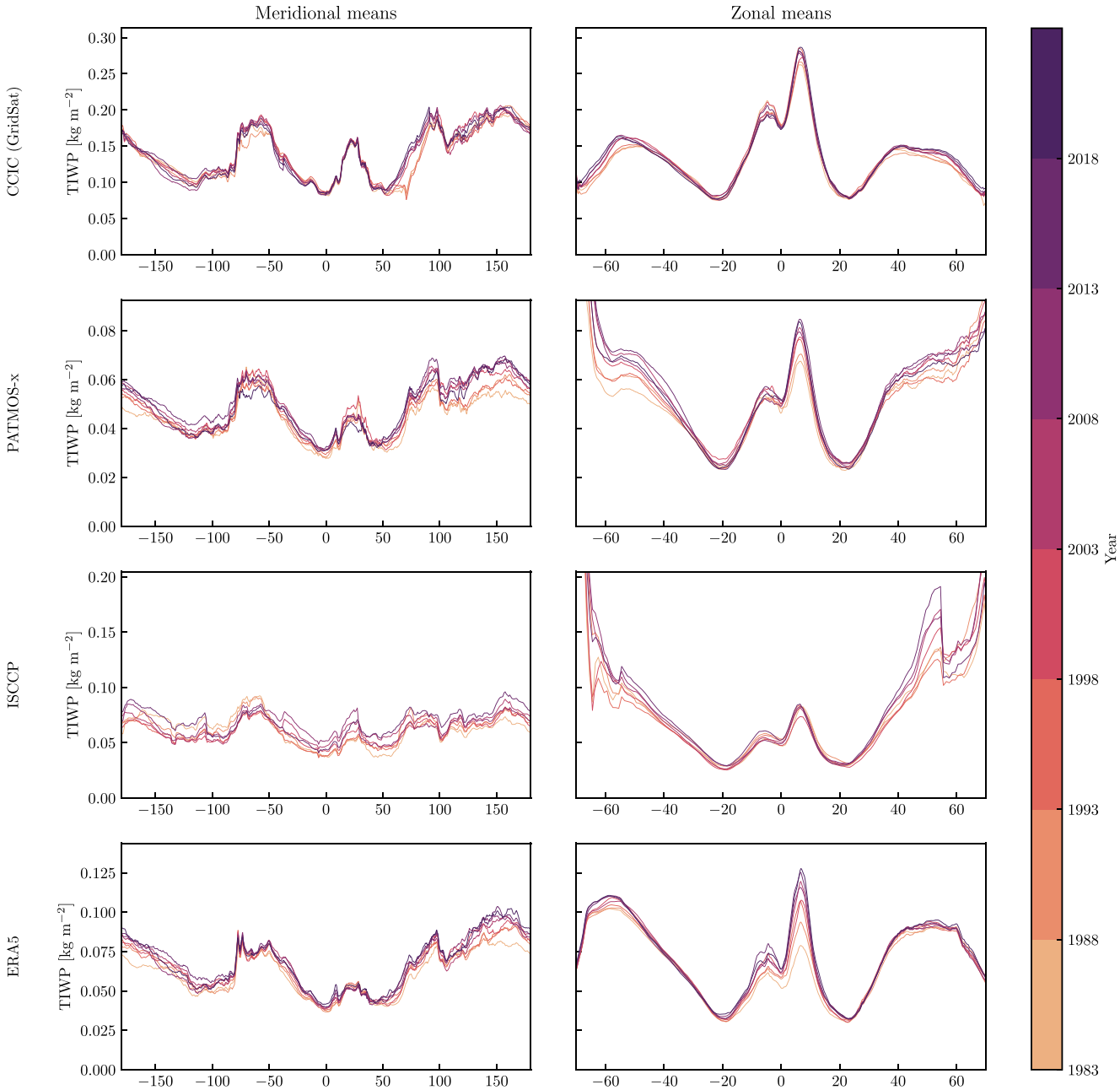

Figure 12. Five-year meridional and zonal means for the long-term TIWP records that covering most of the period 1983 to 2023. Meridional means were area weighted and limited to the latitudes within 70° S and 70° N.

CCIC TIWP estimates are available continuously during both day and night at temporal resolutions 30 min and 3 h, whereas the other records considered here provide estimates only during daytime and, for the MODIS and PATMOS-x records, at lower and irregular temporal sampling.

In terms of robustness, the comparison of the global mean TIWP time series in Figure 6 showed that the CCIC (GridSat) record remains stable from 1983 until the present and does not exhibit any significant discontinuities that may be attributed to changes in the observations system. The CCIC (GridSat) and CCIC (CPCIR) records agree very well up until about the year 2020 after which they seem to diverge slightly. This may be due changes in the input observations in the CPCIR and GridSat input data sets caused by differences between sensor generations. Since the GridSat data set applies the more stringent inter-sensor calibration (K. R. Knapp et al., 2011), this may indicate that the CCIC (GridSat) data set is more suitable for climate applications.

4.2. Comparing Different Long-Term TIWP Records

As has been found in previous studies (Duncan & Eriksson, 2018), currently available TIWP records differ significantly in terms of TIWP magnitudes. This becomes obvious in the time series of global mean TIWP (Figure 6) and the global distributions (Figure 7). Moreover, the zonal means in Figure 8 show that most data sets underestimate the concentrations in the tropics compared to the secondary peaks corresponding to the midlatitude storm tracks. The CCIC records are the only passive sensor-based, long-term TIWP records that are able to reproduce the zonal mean profiles in 2C-ICE. Although the DARDAR zonal means are about 20 % lower than those of 2C-ICE, the CCIC zonal means are still closer to DARDAR than any of the other passive sensor-based data sets. By providing a TIWP record that is consistent with CloudSat-based combined radar/lidar retrievals, CCIC closes an important gap in the observational TIWP record.

In terms of variability, on the other hand, the observational records paint a fairly consistent picture. All observational records agree on the seasonal variability of TIWP in the tropics. The seasonal variability at midlatitudes is also consistent between the data sets while some differences are observed at high latitudes. The tropical seasonal cycle is more intense in the ERA5 data but remains mostly consistent with the purely observational records in terms of the temporal evolution. This is consistent with the findings reported by Duncan & Eriksson, 2018.

4.3. Long-Term Trends

A critical question for long-term records of TIWP is whether they can reliably constrain changes in the global distribution of TIWP. Across the 20 year period during which all records can be compared all data sets except ISCCP show a surprisingly high degree of consistency. Only few areas exhibit statistically significant trends across multiple data sets. These include decreasing trends over the subtropical North Atlantic and increasing trends over the southern Indian Ocean and east of the Hawaiian islands.

For the four data sets allowing trend analysis over 40 years of observations, the observed trend maps show less consistency but highlight larger areas with significant trends. Consistent increasing TIWP trends are observed over the Southern Ocean and the eastern Bering Sea in the CCIC, PATMOS-x, and ERA5 data sets. Although the CCIC (GridSat) record contains artifacts over the Indian Ocean, it appears robust in other regions. In contrast, the ISCCP record shows substantial artifacts and exhibits minimal agreement with the other data sets.

The ERA5 data set aligns somewhat with CCIC (GridSat) results but displays unexpectedly strong trends in the tropics. Notably, ERA5 data indicates a near doubling of TIWP in the ITCZ over 40 years, a magnitude that seems unrealistic. Additionally, the PATMOS-x record demonstrates a bias toward increasing TIWP trends that is not corroborated by the other data sets.

Overall, these results seem to suggest that robust long-term trends remain challenging. Although CCIC (GridSat) exhibits fewer obvious artifacts than ISCCP and less obvious biases than PATMOS-x, it exhibits some artifacts over the Indian Ocean. However, the ERA5 record is not without obvious issues indicating that even reanalysis data sets suffer from the reduced availability and quality of satellite observations during the 80 and 90s.

An important limitation of the CCIC records is that they rely solely on IR cloud top structures to retrieve TIWP. Since the CCIC training data set is derived from almost 4 years of continuous CloudSat/CALIPSO measurements, it will contain a wide range of different cloud scenes covering a wide range of environmental conditions. In principle, this should enable CCIC to detect changes in the distribution of these cloud systems in a changing climate. However, should these changes instead be driven by changes in the internal structure of clouds that are not resolved by the IR observations, CCIC would not be able to detect these changes. Moreover, since the training data for the CCIC is currently limited to the time period 2006–2009, changes in the geostationary input observations caused by generational upgrades outside this period may introduce subtle retrieval errors appearing as spurious trends or masking real ones. The latter issue could be addressed by extending the training period in a potential future update of the data record.

5. Conclusions

This paper introduces CCIC, a novel high-resolution climate record of global frozen hydrometeor concentrations. We evaluate the stability of the record over 40 years by comparing the two versions of the CCIC data set, which are based on different underlying IR measurements, with other existing long-term records of atmospheric cloud

ice, focusing on the total integrated water path (TIWP). First, we validate global TIWP estimates from the various data records against spaceborne radar-lidar measurements from CloudSat and CALIPSO, which serve as the reference for the most accurate cloud ice estimates. Additionally, we compare key spatial and temporal climate variability features captured by the different data sets.

The main findings can be summarized as follows.

- Both CCIC records (GridSat and CPCIR) provide the most accurate currently available TIWP estimates in terms of bias, correlation, and RMSE compared to reference estimates from CloudSat and CALIPSO from instantaneous to monthly timescales.
- The global mean time series of TIWP retrieved from CCIC (CPCIR) and CCIC (GridSat) are stable.
- Quasi-global mean TIWP in CCIC and the CloudSat-based data products 2C-ICE and DARDAR are about three times higher than global estimates from MODIS and PATMOS-x and still more than two times higher than estimates from ISCCP and ERA5.
- Although the absolute global estimates of TIWP differ significantly among the considered data records, these data sets still show good agreement regarding key climate features, such as the seasonal migration of the ITCZ.
- 20 year TIWP trends show good agreement between CCIC, MODIS, PATMOS-x, and ERA5; however, very few regions exhibit significant trends over this time period. Nonetheless, this indicates consistent interannual variability between CCIC, MODIS, PATMOS-x, and ERA5.
- 40 year TIWP trends are less consistent between CCIC, PATMOS-x, ISCCP, and ERA5 but reveal consistent, significant increasing trends present in the CCIC, PATMOS-x, and ERA5 over the Southern Ocean and the Bering sea consistent with a strengthening and poleward movement of the storm tracks. ISCCP 40 year trends are dominated by artifacts. PATMOS-x trends seem biased toward increasing TIWP but show similar patterns as CCIC and ERA5. ERA5 displays an unrealistically strong increase in TIWP in the ITCZ.

The CCIC record is the first deep-learning-based climate record of TIWP. By leveraging a state-of-the-art CNN, CCIC is able to provide TIWP estimates that exceed the accuracy of all existing records at instantaneous and daily timescales and is on par with the MODIS TIWP on monthly timescales despite being based on single-channel IR observations. In contrast to the MODIS and PATMOS-x estimates, the CCIC TIWP is available continuously, that is, during both day and night and at high spatial and temporal resolutions. The CCIC TIWP record thus closes an important gap in the observational record of cloud properties and should be a valuable tool to study various cloud processes and validate high-resolution climate and weather models.

Appendix A: Spatial Mask Applied to Native Time Series

See Figure A1.

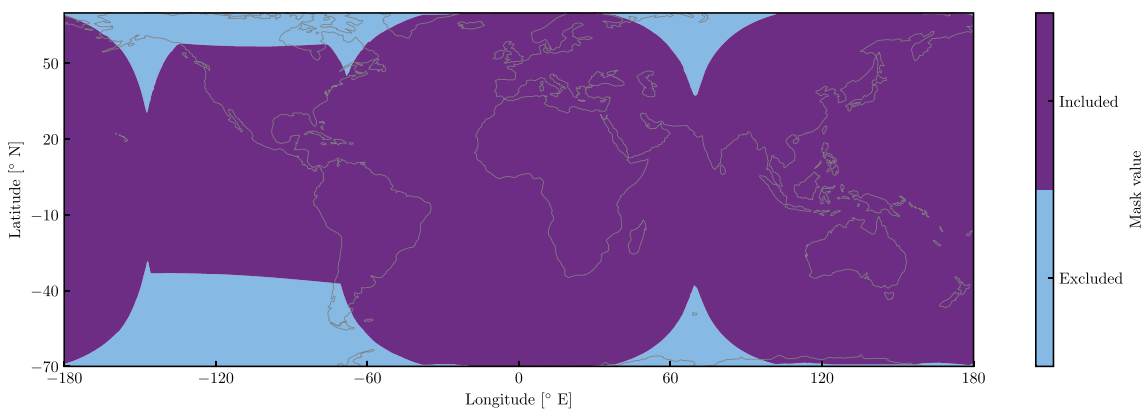

Figure A1. Spatial mask applied to the global means to reduce the impact of spatial sampling on the monthly mean time series. The mask corresponds to the region providing at least 90% valid observations during the first 20 years of the Chalmers Cloud Ice Climatology (GridSat) record.

Data Availability Statement

The full record of the CCIC is publicly available from Amell and Pfreundschuh (2024). The ERA5 reanalysis data set can be downloaded from the Copernicus Climate Data Storage (Copernicus Climate Change Service, 2023). The 2C-ICE (Deng et al., 2024) data and MOD06-1KM-AUX (Cronk & Partain, 2024) data sets were downloaded from the CloudSat Dataprocessing Center. The DARDAR data (Delanoë & Hogan, 2024) was downloaded from the ICARE data center. ISCCP (Rossow, 2024) and PATMOS-x (M. Foster, 2024) data were downloaded from the NOAA National Centers for Environmental Information.

The scripts to download and process each of the data sets and Jupyter Notebooks containing the code for the presented data analysis are available from Pfreundschuh et al. (2024).

Acknowledgments
Julia Kukulies is sponsored by NCAR's Advanced Study Program. The work of Patrick Eriksson and Adrià Amell has been supported in part by the European Union's HORIZON Research and Innovation Programme under grant agreement 101120657, project ENFIELD (European Lighthouse to Manifest Trustworthy and Green AI). The work of Eleanor May and Hanna Hallborn was supported by the Swedish National Space Agency (Grant 2021-00077). The CCIC climate record was created using resources provided by the National Academic Infrastructure for Supercomputing in Sweden (NAISS) partially funded by the Swedish Research Council through grant agreement 2022-06725, Chalmers e-Commons at Chalmers, and Chalmers AI Research Centre. We would like to thank the following data providers: CloudSat Data Processing Center for the 2C-ICE and MOD06-1KM-AUX data products; NASA GES DISC for the CPCIR data; NOAA's National Climatic Data Center for the GridSat data as well as Ken Knapp and colleagues for providing GridSat B1 data set through NOAA'S Climate Data Record program. The results contain modified Copernicus Climate Change Service information 2020. Neither the European Commission nor ECMWF is responsible for any use that may be made of the Copernicus information or data it contains. The computations for this study were performed using several freely available programming languages and software packages, most prominently the Python language (The Python Language Foundation, 2018), the IPython computing environment (Perez & Granger, 2007), the NumPy package for numerical computing (van der Walt et al., 2011), Xarray (Hoyer & Hamman, 2017), and Matplotlib (Hunter, 2007), cmocean (Thyng et al., 2016), seaborn (Waskom, 2021) as well as cartopy (Met Office, 2010 - 2015) for generating figures. The authors thank the two anonymous reviewers who provided valuable guidance to improve the manuscript.

References

Amell, A., & Pfreundschuh, S. (2024). The chalmers cloud ice climatology. Retrieved from https://registry.opendata.aws/ccic/.AmazonWebSevicesOpenData

Amell, A., Pfreundschuh, S., & Eriksson, P. (2024). The chalmers cloud ice climatology: Retrieval implementation and validation. *Atmospheric Measurement Techniques*, *17*(14), 4337–4368. https://doi.org/10.5194/amt-17-4337-2024

Bony, S., Stevens, B., Frierson, D. M. W., Jakob, C., Kageyama, M., Pincus, R., et al. (2015). Clouds, circulation and climate sensitivity. *Nature Geoscience*, *8*(4), 261–268. Retrieved from https://doi.org/10.1038/ngeo2398

Chen, T., Rossow, W. B., & Zhang, Y. (2000). Radiative effects of cloud-type variations. *Journal of Climate*, *13*(1), 264–286. Retrieved from https://doi.org/10.1175/1520-0442(2000)013⟨0264:REOCTV⟩2.0.CO;2

CloudSat Project. (2018). Cloudsat mod06-aux auxiliary data. *CloudSat Data Processing Center*.

Copernicus Climate Change Service. (2023). Era5 hourly data on slingle levels from 1940 to present [dataset]. *Copernicus Climate Change Service (C3S) Climate Data Store (CDS)*. https://doi.org/10.24381/cds.adbb2d47

Cronk, H., & Partain, P. (2024). Mod06-1km-aux [dataset]. Retrieved from https://www.cloudsat.cira.colostate.edu/data-products/mod06-1km-aux.CloudSatDataProcessingCenter. accessed 01 08 2024.

Delanoë, J., & Hogan, J. R. (2024). Dardar cloud [dataset]. Retrieved from https://www.icare.univ-lille.fr/dardar/overview-dardar-cloud/.AERIS/ICAREDataandServicesCenter. accessed 01 08 2024.

Delanoë, J., & Hogan, R. J. (2010). Combined cloudsat-calipso-modis retrievals of the properties of ice clouds. *Journal of Geophysical Research*, *115*(D4). https://doi.org/10.1029/2009JD012346

Deng, M., Mace, G. G., Wang, Z., & Berry, E. (2015). Cloudsat 2c-ice product update with a new ze parameterization in lidar-only region. *Journal of Geophysical Research: Atmospheres*, *120*(23), 12198–12208. https://doi.org/10.1002/2015JD023600

Deng, M., Mace, G. G., Wang, Z., & Berry, E. (2024). 2c-ice p1_r05 [dataset]. Retrieved from https://www.cloudsat.cira.colostate.edu/data-products/2c-ice.CloudSatDataProcessingCenter. accessed 01 08 2024.

Duncan, D. I., & Eriksson, P. (2018). An update on global atmospheric ice estimates from satellite observations and reanalyses. *Atmospheric Chemistry and Physics*, *18*(15), 11205–11219. Retrieved from https://doi.org/10.5194/acp-18-11205-2018

Eliasson, S., Buehler, S. A., Milz, M., Eriksson, P., & John, V. O. (2011). Assessing observed and modelled spatial distributions of ice water path using satellite data. *Atmospheric Chemistry and Physics*, *11*(1), 375–391. Retrieved from https://doi.org/10.5194/acp-11-375-2011

Feng, Z., Leung, L. R., Hardin, J., Terai, C. R., Song, F., & Caldwell, P. (2023). Mesoscale convective systems in dyamond global convection-permitting simulations. *Geophysical Research Letters*, *50*(4), e2022GL102603. https://doi.org/10.1029/2022gl102603

Foster, M. (2024). Patmos-x cloud properties cdr [dataset]. NOAA National Centers for Environmental Information. https://doi.org/10.7289/V5X9287S

Foster, M. J., Phillips, C., & Heidinger, A. K., & NOAA CDR PROGRAM. (2021). Noaa climate data record (cdr) of advanced very high resolution radiometer (avhrr) and high-resolution infra-red sounder (hirs) reflectance, brightness temperature, and cloud products from pathfinder atmospheres - Extended (patmos-x). version 6.0. *NOAA National Centers for Environmental Information*. https://doi.org/10.7289/V5X9287S

Foster, M. J., Phillips, C., Heidinger, A. K., Borbas, E. E., Li, Y., Menzel, W. P., et al. (2023). Patmos-x version 6.0: 40 years of merged avhrr and hirs global cloud data. *Journal of Climate*, *36*(4), 1143–1160. https://doi.org/10.1175/jcli-d-22-0147.1

Hersbach, H., Bell, B., Berrisford, P., Hirahara, S., Horányi, A., Muñoz-Sabater, J., et al. (2020). The era5 global reanalysis. *Quarterly Journal of the Royal Meteorological Society*, *146*(730), 1999–2049. https://doi.org/10.1002/qj.3803

Hoyer, S., & Hamman, J. (2017). xarray: N-D labeled arrays and datasets in Python. *Journal of Open Research Software*, *5*(1), 10. Retrieved from https://doi.org/10.5334/jors.148

Hunter, J. D. (2007). Matplotlib: A 2d graphics environment. *Computing in Science and Engineering*, *9*(3), 90–95. https://doi.org/10.1109/MCSE.2007.55

Janowiak, J. E., Joyce, B., & Xie, P. (2017). *Ncep/cpc l3 half hourly 4km global (60s - 60n) merged ir v1*. Goddard Earth Sciences Data and Information Services Center (GES DISC). https://doi.org/10.5067/P4HZB9N27EKU

Janowiak, J. E., Joyce, R. J., & Yarosh, Y. (2001). A real-time global half-hourly pixel-resolution infrared dataset and its applications. *Bulletin of the American Meteorological Society*, *82*(2), 205–218. https://doi.org/10.1175/1520-0477(2001)082⟨0205:ARTGHH⟩2.3.CO;2

Knapp, K. R., Ansari, S., Bain, C. L., Bourassa, M. A., Dickinson, M. J., Funk, C., et al. (2011). Globally gridded satellite observations for climate studies. *Bulletin of the American Meteorological Society*, *92*(7), 893–907. https://doi.org/10.1175/2011BAMS3039.1

Knapp, W. B. A. W., Golea, V., Knapp, K. R., Young, A., & Inamdar, A., & NOAA's Climate Data Record Program. (2016). International satellite cloud climatology project climate data record, h-series [hgm, hgg]. *NOAA National Centers for Environmental Information*. https://doi.org/10.7289/V5QZ281S

Lucas-Picher, P., Argüeso, D., Brisson, E., Tramblay, Y., Berg, P., Lemonsu, A., et al. (2021). Convection-permitting modeling with regional climate models: Latest developments and next steps. *Wiley Interdisciplinary Reviews: Climate Change*, *12*(6), e731. https://doi.org/10.1002/wcc.731

Met Office. (2010) - 2015. Cartopy: A cartographic python library with a matplotlib interface [Computer software manual]. *Exeter, Devon*. Retrieved from http://scitools.org.uk/cartopy

Perez, F., & Granger, B. E. (2007). Ipython: A system for interactive scientific computing. *Computing in Science & Engineering*, *9*(3), 21–29. https://doi.org/10.1109/MCSE.2007.53

Pfreundschuh, S., J, K., Amell, A., Hallborn, H., May, E., & Eriksson, P. (2024). SEE-GEO/ccic_climate_record_analysis [dataset]. *Zenodo*. Retrieved from https://doi.org/10.5281/zenodo.13871514

Platnick, S. (2019). Modis atmosphere l3 cloud properties product. version-1.1. *NASA Level-1 and Atmosphere Archive & Distribution System (LAADS) Distributed Active Archive Center (DAAC)*. https://doi.org/10.5067/MODIS/CLDPROP_M3_MODIS_Aqua.011

Platnick, S., Meyer, K. G., King, M. D., Wind, G., Amarasinghe, N., Marchant, B., et al. (2016). The modis cloud optical and microphysical products: Collection 6 updates and examples from terra and aqua. *IEEE Transactions on Geoscience and Remote Sensing*, *55*(1), 502–525. https://doi.org/10.1109/tgrs.2016.2610522

Prein, A. F., Langhans, W., Fosser, G., Ferrone, A., Ban, N., Goergen, K., et al. (2015). A review on regional convection-permitting climate modeling: Demonstrations, prospects, and challenges. *Reviews of Geophysics*, *53*(2), 323–361. https://doi.org/10.1002/2014rg000475

Rossow, W. B. (2024). Isccp h-series cdr [dataset]. NOAA National Centers for Environmental Information. https://doi.org/10.7289/V5QZ281S

Rossow, W. B., & Schiffer, R. A. (1999). Advances in understanding clouds from isccp. *Bulletin of the American Meteorological Society*, *80*(11), 2261–2288. https://doi.org/10.1175/1520-0477(1999)080<2261:aiucfi>2.0.co;2

Stephens, G. L., Vane, D. G., Boain, R. J., Mace, G. G., Sassen, K., Wang, Z., et al. (2002). The cloudsat mission and the a-train: A new dimension of space-based observations of clouds and precipitation. *Bulletin of the American Meteorological Society*, *83*(12), 1771–1790. https://doi.org/10.1175/bams-83-12-1771

The Python Language Foundation. (2018). The python language reference. Retrieved from https://docs.python.org/3/reference/index.html

Thyng, K. M., Greene, C. A., Hetland, R. D., Zimmerle, H. M., & DiMarco, S. F. (2016). True colors of oceanography: Guidelines for effective and accurate colormap selection. *Oceanography*, *29*(3), 9–13. https://doi.org/10.5670/oceanog.2016.66

Turbeville, S., Nugent, J., Ackerman, T., Bretherton, C., & Blossey, P. (2022). Tropical cirrus in global storm-resolving models: 2. Cirrus life cycle and top-of-atmosphere radiative fluxes. *Earth and Space Science*, *9*(2), e2021EA001978. https://doi.org/10.1029/2021ea001978

van der Walt, S., Colbert, S. C., & Varoquaux, G. (2011). The numpy array: A structure for efficient numerical computation. *Computing in Science & Engineering*, *13*(2), 22–30. https://doi.org/10.1109/MCSE.2011.37

Waliser, D. E., Li, J.-L. F., Woods, C. P., Austin, R. T., Bacmeister, J., Chern, J., et al. (2009). Cloud ice: A climate model challenge with signs and expectations of progress. *Journal of Geophysical Research*, *114*(D8). Retrieved from https://doi.org/10.1029/2008JD010015

Waskom, M. L. (2021). seaborn: Statistical data visualization. *Journal of Open Source Software*, *6*(60), 3021. Retrieved from https://doi.org/10.21105/joss.03021